Impact of Assimilating Passive Microwave Observations on Root-Zone Soil Moisture Under Dynamic Vegetation Conditions

Karthik Nagarajan, *Member, IEEE*, Jasmeet Judge, *Senior Member, IEEE*, Alejandro Monsivais-Huertero, and Wendy D. Graham

***Abstract*—In this paper, L-band microwave observations were assimilated using the ensemble Kalman filter to improve root-zone soil moisture (RZSM) estimates from a coupled soil vegetation atmosphere transfer (SVAT)-vegetation model linked to a forward microwave model. Simultaneous state-parameter updates were performed by assimilating both synthetic and field observations during a growing season of sweet corn every three days, matching the temporal coverage of observations from the Soil Moisture and Ocean Salinity and Soil Moisture Active Passive missions. The sensitivities of parameters to the states were investigated using the information-theoretic measure of conditional entropy. Among the soil parameters, the pore-size index (λ) was the most sensitive to brightness temperatures (T_B) during the early and midgrowth stages, while porosity (ϕ) was the most sensitive to T_B during the reproductive stage. In the microwave model, the soil roughness parameters, root mean square (RMS) height (r), and correlation length (l) were the most sensitive during the early and mid stages, while the vegetation regression parameter (b) was the most sensitive during the reproductive stage. In the synthetic experiment, assimilation of T_B provided RMS error reductions in RZSM estimates of 70% compared to open loop estimates. Minimal variations in performance were observed across different stages of the season during the synthetic experiment. However, when field observations of T_B were assimilated, significant differences in RZSM estimates were observed during different growth stages. Maximum RMS difference (RMSD) reductions in RZSM estimates of 33.3% were observed compared to open loop estimates during the early stages, while improvements of 4.8% and 16.7% were observed in the mid- and reproductive stages, respectively. Further analyses of assimilation with field observations also suggest some improvements in the SVAT model are needed for moisture transport immediately following the precipitation/irrigation events. In the microwave model, the linear vegetation formulation for estimating canopy opacity, parameterized by b, was inadequate in capturing the complexities in T_B during stages of high vegetative and reproductive growth rates.**

Manuscript received November 8, 2010; revised June 10, 2011 and October 28, 2011; accepted February 24, 2012. Date of publication June 6, 2012; date of current version October 24, 2012. This work was supported by the NASA-Terrestrial Hydrology Program (THP)-NNX09AK29G. Partial support for MicroWEX-5 was obtained from the NSF Earth Science Division (EAR-0337277) and the NASA New Investigator Program (NASA-NIP-00050655).

K. Nagarajan and J. Judge are with the Center for Remote Sensing, Agricultural and Biological Engineering Department, Institute of Food and Agricultural Sciences, University of Florida, Gainesville, FL 32611 USA (e-mail: nagkart@ufl.edu; jasmeet@ufl.edu).

A. Monsivais-Huertero is with the ESIME Unidad Ticoman, Insitituto Policnico Nacional, 07738 Mexico, DF, Mexico (e-mail: monsivais@ufl.edu).

W. D. Graham is with the Water Institute, University of Florida, Gainesville, FL 32611 USA (e-mail: wgraham@ufl.edu).

Color versions of one or more of the figures in this paper are available online at http://ieeexplore.ieee.org.

Digital Object Identifier 10.1109/TGRS.2012.2191154

***Index Terms*—Conditional entropy (CH), dynamic vegetation, Ensemble Kalman Filter (EnKF), parameter sensitivity, passive microwave assimilation, root-zone soil moisture (RZSM).**

I. Introduction

MICROWAVE signatures at frequencies <10 GHz are highly sensitive to changes in soil moisture at the top few centimeters (near-surface). Accurate knowledge of root-zone soil moisture (RZSM) is essential for near-term climate predictions, hydrologic, and agricultural research [1], and for effective water resources management. The near-surface soil moisture can be linked to RZSM through soil vegetation atmosphere transfer (SVAT) models. These models can be coupled with vegetation growth models to estimate RZSM under dynamic vegetation conditions. However, the coupled models exhibit large uncertainties in their RZSM estimates due to accumulation of errors in model formulation, computation, initialization, and forcings, and due to unresolved heterogeneity in model parameters. Such uncertainties can be reduced by assimilating microwave observations directly into SVAT-vegetation models that are linked to forward microwave models [2], [3]. The European Space Agency-Soil Moisture and Ocean Salinity [4] and the near-future NASA-Soil Moisture Active Passive missions [5], [6] will provide unprecedented observations of brightness temperatures (T_B) at 1.4 GHz for soil moisture research, and therefore it is important to understand and evaluate the impact of using T_B in the estimation of RZSM.

Ensemble-based assimilation techniques such as the ensemble Kalman filter (EnKF) are efficient for land data assimilation research and applications since they can be applied to nonlinear and discontinuous models [7]. In particular, the EnKF has emerged as the algorithm of choice for soil moisture data assimilation in many studies [2], [8]–[14]. However, only a few studies have included EnKF-based assimilation of L-band microwave brightness temperatures to improve RZSM estimates. Most of these studies have involved assimilation of near-surface soil moisture that is derived empirically from synthetic observations of T_B either under static vegetation or bare soil conditions [15]–[17]. Even fewer studies have utilized real observations of T_B [3], [18], [19] by retrieving soil moisture values from observed T_B and assimilating the retrieved values into an SVAT model. Studies that assimilate observations of T_B to improve RZSM estimates by linking SVAT models to forward microwave models are very few and are primarily

synthetic studies [20]. Assimilation of both synthetic and field observations of T_B are necessary to understand the impact of uncertainties in model biophysics, particularly under dynamic vegetation conditions.

Simultaneous update of states and parameters using EnKF provide more accurate RZSM estimates in terms of reducing the root mean square error (RMSE) compared to state-only updates when observations of volumetric soil moisture (VSM) at depths of 2 and 4 cm were assimilated [8], [21]. Simultaneous estimation of parameters with states can also be used for addressing bias in models that is not removed by the EnKF [22]. This is important because, while the observations typically follow model physics closely in the so-called identical twin synthetic studies, additional bias may be introduced when field observations are assimilated, particularly under dynamic land-surface conditions. Since parameters affect the accuracy of RZSM estimates, analyses of the impacts of updating different parameters in both the SVAT and the microwave model on RZSM estimates are needed. To our knowledge, studies involving simultaneous update of states and parameters have not yet been performed when observations of T_B are directly assimilated into a forward microwave model. Not all parameters in the SVAT and microwave models are sensitive to the RZSM or T_B observations. According to the hypothesis of equifinality [23], estimating states and parameters from observations of T_B imposes an inverse problem wherein multiple parameter combinations may offer similar RZSM estimates. Unless necessary steps are taken to identify and include only the most sensitive parameters to T_B and VSM during assimilation, the updates can either prove ineffective due to equifinality or cause instabilities in the EnKF performance [24]. Reducing the number of parameters in the update process is also desirable to reduce computational complexity. In the past, sensitivity studies based on second-order statistics such as correlation have been used to select the parameters most sensitive to VSM in an SVAT model [8]. However, measures that capture information from higher order moments, such as conditional entropy (CH) from information theory may be required to analyze the sensitivity of SVAT model parameters to T_B due to the nonlinear relationship between VSM and T_B.

The primary goal of this study is to understand the impact of assimilating T_B observations on RZSM estimation. Synthetic and field observations of T_B from our fifth Microwave Water Energy Balance Experiment (MicroWEX-5) are assimilated every three days in a coupled SVAT-vegetation model linked with a forward microwave model during a growing season of sweet corn in North Central Florida. The synthetic observations are used to conduct a comparative study on two sets of assimilation experiments: 1) simultaneous estimation of states and parameters; and 2) simultaneous estimation of states and a reduced set of the most sensitive parameters. The results from the synthetic experiment are also compared to those using field observations obtained during the MicroWEX-5. Parameter convergence and errors in T_B and RZSM estimates are analyzed over different growth stages of the sweet corn season to understand the seasonal impact of assimilation and to investigate the model biophysics and the bias between the model and the observations.

TABLE I
GROWTH STAGES OF SWEET CORN DURING THE MICROWEX-5 FROM [36]

Stage	DoY	Height (cm)	LAI	Characteristics
Early	70-95	< 34	< 0.35	Almost bare soil; emergence DoY 72
Mid	96-115	$34 - 120$	$0.35 - 2.0$	Maximum vegetative growth; tasseling on DoY 109
Reproductive	116-142	$120 - 192$	$2.0 - 2.4$	Silking on DoY 115; ear formation on DoY 121

In the next section, we briefly describe the MicroWEX-5 observations and the coupled SVAT-Vegetation-passive microwave model, the CH used for parameter sensitivity and the EnKF algorithm.

II. EXPERIMENT, MODELS, AND ALGORITHMS

A. Fifth Microwave Water Energy Balance Experiment (MicroWEX-5)

The MicroWEX-5 was conducted during a growing season of sweet corn from Day of Year (DoY) 68 (March 9) to DoY 150 (May 30) in 2006, to monitor micrometeorological, soil, and vegetation conditions as well as the horizontally polarized microwave brightness temperatures at L-band [25]. The experimental site is a 3.6 hectare (9 acre) field located at the UF/IFAS Plant Science and Research Education Unit, in North Central Florida (29.41 N, 82.18 W). The soils at the site are lake fine sand, with 89.4% sand, 7.1% clay, and a bulk density of 1.55 g/cm^3. Corn was planted at a row spacing of 76 cm, with a density of 8 plants/m^2. Observations used in this study include every 15-min measurements of VSM, wind speed at 1.8 m, upwelling and downwelling short and longwave radiation, precipitation/irrigation, relative humidity, and air temperature at 2.66 m. The soil moisture values were observed at depths of 2, 4, 8, 16, 32, 64, and 100 cm, using Campbell Scientific Water Content Reflectometers. Four tipping-bucket rain gauges logged precipitation and irrigation at four locations in the field. Table I shows the different growth stages of corn and their associated vegetation characteristics observed during MicroWEX-5. Observations of T_B at 1.4 GHz were also collected at 15-min intervals using the University of Florida L-band Microwave Radiometer. The 3-dB bandwidth and beamwidth of the radiometer were 20 MHz and 22.5°, respectively, and the noise figure and RF gain were 3.99 dB and 79 dB, respectively.

B. Coupled LSP-DSSAT Model

The Land Surface Process (LSP) model [26] is an SVAT model that simulates 1-D coupled energy and moisture transport in soil and vegetation, and estimates energy and moisture fluxes at the land surface and in the vadose zone. The model has been rigorously tested [26], [27] and extended to wheat-stubble [28] and brome-grass in the Great Plains, prairie wetlands in Florida [29], and to tundra in the Arctic [30]. The vegetation energy balance is calculated using [31] for the water drainage from canopy, the bulk transfer approach for the sensible heat flux from [32], and the latent heat flux

TABLE II
PARAMETERS INCLUDED IN THE LSP-DSSAT MODEL [36]. THE VALUES FOR CANOPY PARAMETERS WERE FROM [72], AND RANGES FOR SOIL PARAMETERS WERE FROM [73]

	Parameter	Description	Values
CANOPY	z_{ob}	Bare soil roughness length (m)	0.004
	x	Leaf angle distribution parameter	0.819
	σ	Leaf reflectance	0.474
	ϵ_c	Canopy emissivity	0.973
	ϵ_s	Soil emissivity	0.953
	c_d	Canopy drag coefficient	0.328
	i_w	Canopy wind intensity factor	67.9
	l_w	Leaf width (m)	0.0531
	F_b	Base assimilation rate (kg CO_2/m^2s)	$-0.82X10^{-8}$
	ϵ_{photo}	Photosynthetic efficiency (kg CO_2/J)	$0.897X10^{-6}$
	$soil_a$	Slope parameter for r_s (m^2s/kg H_2O)	370
	$soil_b$	Intercept parameter for r_s (m^2s/kg H_2O)	-531
SOIL (0-1.7 m)	λ	Pore-size index	$0.1-0.9$
	ψ_0	Air entry pressure (m H_2O)	$0.05-1.0$
	K_{sat}	Saturated hydraulic conductivity (m/s)	$10^{-5}-10^{-3}$
	ϕ	Porosity (m^3/m^3)	$0.2-0.55$
SOIL (1.7-2.7 m)	λ	Pore-size index	0.05
	ψ_0	Air entry pressure (m H_2O)	0.019
	K_{sat}	Saturated hydraulic conductivity (m/s)	$8.93X10^{-5}$
	ϕ	Porosity (m^3/m^3)	0.41
CULTIVAR	$P1$	Degree days between emergence and end of juvenile stage	157.20
	$P2$	Development delay for each hour increase in photoperiod past optimum photoperiod	1.00
	$P5$	Degree days from silking to maturity	811.20
	$G2$	Maximum possible number of kernels per plant	853.00
	$G3$	Kernel filling rate during the linear grain filling stage and under optimum conditions (mg/d)	10.40
	$PHINT$	Phyllochron interval	40.33

following [33]. The coupled energy and water balance in soil is calculated from [34] and [35]. A block-centered finite-difference scheme is employed to solve the coupled governing equations at an adaptive time step (s/min) in response to the forcings [36]. The LSP model has been coupled with a widely used crop-growth model, viz Decision Support System for Agrotechnology Transfer (DSSAT) that simulates daily crop growth (biomass accumulation) and development (vegetative and reproductive growth stages) for a variety of crops such as corn, soybeans, wheat, and cotton [37] when forced with meteorological conditions. The soil module in DSSAT simulates soil water transport using the Bucket model (Manabe, 1969) and soil temperature as an empirical function of air temperature and depth. The soil-plant-atmosphere module estimates evotranspiration (ET). CERES-Maize [38] is a part of the crop growth submodule that simulates corn growth and development. The model incorporates management such as irrigation, fertilization, and pesticide applications. The calibrated values of the six cultivar coefficients that describe growth and development characteristics for different maize cultivars, are given in Table II, as obtained from [36]. The DSSAT model has been extensively tested in different hydroclimatic regions [37], [39]–[47], including North-Central Florida [48]. In the coupled LSP-DSSAT model, at the end of each day of simulation, the LSP model provides the DSSAT model with estimates of soil moisture and soil temperature profiles and ET and the DSSAT model provides the LSP model with vegetation characteristics such as vegetation water content (VWC), biomass, and plant height and width that influence heat, moisture, and radiation transfer at the land surface [36].

C. Microwave Brightness (MB) Model

The MB model is the widely used $\tau-\omega$ model [49]. A vegetated surface is modeled as a single isothermal layer of vegetation with diffuse boundaries over a soil half-space [50]. The soil moisture and temperature profiles provided by the LSP model and the leaf/ear biomass, VWC, and plant height provided by the DSSAT model are used by the MB model in simulating brightness temperature. Using a zeroth-order radiative transfer approach, the total brightness temperature of a terrain (T_B) is the sum of contributions from soil $(T_{Bsoil,p})$, vegetation $(T_{Bcanopy,p})$, and from sky $(T_{Bsky,p})$

$$\begin{aligned} T_{Bsoil,p} &= (1-r_p)T_{eff}exp\left(-\frac{\tau}{\mu}\right) \\ T_{Bcanopy,p} &= T_c\left[1-exp\left(-\frac{\tau}{\mu}\right)\right](1-\omega)\left[1+r_p exp\left(-\frac{\tau}{\mu}\right)\right] \\ T_{Bsky,p} &= T_{sky}r_p exp\left(-\frac{2\tau}{\mu}\right) \end{aligned} \quad (1)$$

where p is the polarization, r_p is the reflectivity of the rough soil surface, T_{eff} is the effective radiating temperature of the soil, $\mu = cos\theta$, where θ is the incidence angle, T_c is the physical temperature of the isothermal canopy, ω is the single scattering albedo, τ is the optical depth, and T_{sky} is the downwelling sky brightness.

The θ was set to 50° in this study to match the incidence angle for the MicroWEX-5 observations. T_{sky} was set to 5 K [49] and r_p was obtained by integrating the bistatic scattering coefficient from the IEM model [51]. The soil dielectric properties were obtained from the four-component model described in [52].

The optical depth was calculated from the linear relationship $\tau = b * VWC$ [53], where b is a regression coefficient that depends upon canopy, frequency, and polarization. This linear dependency of optical depth on VWC has been confirmed by [54], [55], with a range of b values for a single crop. In general, the variation in b reduces for low frequencies, such as 0.1–0.3 for frequencies lower than 3 GHz [54].

D. Conditional Entropy

In this paper, we employ an information-theoretic measure known as CH to identify the parameters most sensitive to T_B. Statistical measures such as correlation include only second-order moments and may provide reduced information on sensitivities under dynamic vegetation conditions. Information-theoretic measures [56], such as CH, quantify the stochastic structure of data beyond second-order statistics by embedding information from the complete probability density function (PDF). In an information-theoretic framework, a parameter is said to be sensitive to T_B or RZSM if it provides a good separation among different classes of T_B or RZSM, where the classes represent different ranges of T_B or RZSM values. The CH metric offers a quantitative way of measuring this separation [57]. The CH for a set of classes w given a particular feature F_i is represented as $CH(w|F_i)$ and is computed using

$$CH(w|F_i) = -\sum_{F_i} p(F_i) \sum_{w} p(w|F_i) log\left[p(w|F_i)\right]$$

$$= \sum_{w,F_i} p(w,F_i) log \frac{p(F_i)}{p(w,F_i)}. \tag{2}$$

Given a set of parameters $F = F_1, F_2, \ldots, F_m$ and a vector of T_B classes w, the set of parameters within F that are most sensitive to T_B is the set that provides the smallest value for CH.

To estimate the PDFs, $p(F_i)$ and $p(w, F_i)$, in (2), a nonparametric PDF estimation technique known as Parzen windows [58] will be used. In this technique, symmetric functions, known as kernels, are used to estimate the PDF of a random variable based on a finite set of data samples. The Kernels assign weights to each of the samples based upon their distance from the point at which the PDF is estimated, with higher weights being assigned to the samples that are closer to the point. In this paper, a zero-mean, unity-variance Gaussian function will be used as the kernel. With Gaussian kernels, the weight decreases exponentially with the square of the distance, rendering the distant points irrelevant.

Given n samples of the feature F_i ($F_{i,j}$, $j = [1, 2, \ldots, n]$), the probability of F_i at a point F_i^k is represented as $p(F_i = F_i^k)$ and computed using (3) where $k = [1, 2, \ldots, M]$ represents the M discrete points at which the PDF is estimated

$$p\left(F_i = F_i^k\right) = \frac{1}{n} \sum_{j=1}^{n} \frac{1}{h} \psi \left(\frac{F_i^k - F_{i,j}}{h} \right) \tag{3}$$

where ψ is the Gaussian kernel and h is a smoothing parameter, which relates to the variance in ψ. The parameter h will be determined based on Silverman's rule, which is a standard rule-of-thumb that is used in kernel-based estimation algorithms [59], as given in (4). The PDF $p(w, F_i)$ is a 2-D PDF that will be computed at M^2 points, similar to that of $p(F_i)$

$$h = 1.06 min \left[\sigma, \frac{I_{QR}}{1.34}\right] n^{-\frac{1}{5}} \tag{4}$$

where σ and I_{QR} are the standard deviation and inter-quartile range, respectively, computed from the n samples.

E. Ensemble Kalman Filter

In the EnKF, a set of ensemble members representing state vectors is propagated in parallel, such that each state vector represents one realization of a nonlinear model. The state equation for each ensemble member in the filter is [60]

$$x_t^{i-} = f\left(x_{t-1}^{i+}, u_{t-1}^i, \theta_{t-1}^{i+}, t-1\right) + \eta_{t-1}^i \tag{5}$$

where $f(\cdot)$ is the nonlinear model, x_t^{i-} is the state of the ith ensemble member prior to the update at time t, x_{t-1}^{i+} is the posterior state of the ith ensemble member at time $t-1$, u_{t-1}^i represents the meteorological forcings and other inputs, θ_{t-1}^+ represents the model parameters, and η_{t-1}^i is the model error. In our study, the model physics are assumed to be perfect ($\eta_{t-1}^i = 0$).

The observation equation given in (6) relates the prior state (x^{i-}) to the observations (d^i) through the measurement operator h, perturbed by errors associated with the observations, ϵ, at time t

$$d_t^i = h x_t^{i-} + \epsilon_t^i \tag{6}$$

where ϵ is the error associated to the observations and is assumed to be Gaussian with zero mean and variance R in this work.

The ensemble of state vectors x^i and perturbed observations d^i can be represented in matrix form as

$$A = \{x^1, x^2, \ldots, x^N\} \tag{7}$$

$$D = \{d^1, d^2, \ldots, d^N\} \tag{8}$$

where N is the number of ensemble members.

The posterior matrix of state vectors A_t^+ is computed as a linear combination of the prior estimate A_t^- and the observation vector D_t weighed by the Kalman gain K_t

$$A_t^+ = A_t^- + K_t\left(D_t - H A_t^-\right) \tag{9}$$

where H is the operator relating the ensemble of perturbated observations to the ensemble of states.

The Kalman gain can be calculated as [61]

$$K = P_x H^T \left(H P_x H^T + R_e\right)^{-1} \tag{10}$$

where P_x represents the prior state covariance matrix, and R_e is the covariance matrix of the observation errors.

III. Methodology

In this section, we describe the LSP-DSSAT-MB simulations and the implementation of the EnKF algorithm for our study. The model integration and assimilation set up is shown in Fig. 1.

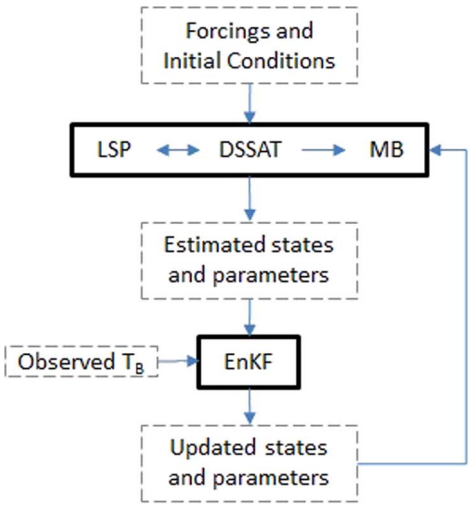

Fig. 1. Model integration and assimilation setup.

A. LSP-DSSAT-MB Simulations

Model simulations using the LSP-DSSAT-MB model were conducted from planting on DoY 68, to harvest on DoY 142, in 2006 during MicroWEX-5. Micrometeorological forcings and vegetation properties for the simulations were obtained from the MicroWEX-5 and DSSAT, respectively. Initial moisture and temperature conditions were obtained from the first values observed by the soil moisture and temperature sensors on DoY 72, three days after planting. Initializations at depths where observations were not available including the lower boundary were set via interpolation. Initialization errors in soil moisture and temperature profiles were assumed to be zero because the soil was heavily irrigated after planting leading to near-saturated conditions, when initialization uncertainties have negligible impacts on soil moisture and soil temperature estimates, similar to [62]. At the field site, the first 1.7 m of soil was primarily sandy, with volumetric sand fraction of 0.894 and the second layer (1.7–2.7 m), with the fraction of 0.405. In the LSP model, the soil was discretized into 35 computational blocks in the two layers with different constitutive properties. The blocks increased in thickness exponentially, with four blocks in the top 5 cm of the soil. The LSP model includes 16 parameters as shown in Table II. The constitutive properties of the first layer of the soil were estimated during assimilation, as explained in Section III-C. The second layer (1.7–2.7 m) of the soil was assumed to have known constitutive properties, obtained from [36], as shown in Table II.

B. Sensitivity of Parameters to RZSM and T_B

As mentioned before, the augmented state vector technique [8], [21] is applied to simultaneously update states and parameters using EnKF in this study. To determine the parameters most sensitive to T_B, the correlation coefficients (CC) and CH are computed between the parameters and open loop simulations of RZSM and T_B over the entire growing season. The four soil parameters in the LSP model-porosity (ϕ), air entry pressure (ψ_0), pore-size index (λ), and saturated hydraulic conductivity (K_{sat}) and additional four parameters in the MB model: RMS height (r), correlation length (l), the vegetation parameter, b, and the scattering coefficient (ω) are considered in this study. The LSP parameters in Table III were found to be the most influential for RZSM estimation, based upon time-dependent correlations of the RZSM estimates to the 16 parameters in the LSP model [8], [63]. MB model parameters related to soil roughness and canopy were also used in this study. The soil roughness is the most influential in estimating T_B contribution from the soil. Past studies have investigated multiple parameterizations to describe the soil roughness. While microwave signatures were found to be sensitive to changes in r only in [64], another study [65] proposed the inclusion of a third parameter in addition to r and l. In this paper, we included both r and l in the state vector and assumed them to independently describe the soil surface. The b parameter is the only canopy-related parameter in the MB model, and was included in the state vector. All the parameters are randomly generated from uniform distributions with literature-based upper and lower bounds (see Table III). The use of a uniform distribution avoids the generation of negative parameters and assumes that all values are equally likely. In computing the CH, the eight parameters in Table III represent the features $F_1, F_2, \ldots, F_8$ and the PDFs $p(F_i)$ and $p(w, F_i)$ are estimated considering $M = 8$ using Parzen windows. The entropy of a PDF is maximum when the PDF is uniformly distributed, which in this case corresponds to $p(w = w_k|F_i) = 1/8$ for $k = 1, 2, \ldots, 8$. Therefore, the largest CH value that can be obtained in separating eight classes of T_B or RZSM is 2.07 nats or $ln(8)$. A nat is a logarithmic unit of information based on natural logarithms and powers of e.

TABLE III
PARAMETERS IN THE LSP AND MB MODEL CONSIDERED FOR UPDATE DURING ASSIMILATION. THE RANGES OF PARAMETERS IN THE MB MODEL WERE OBTAINED FROM [51], [64]

Parameter	Description	Ranges
λ	Pore-size index	$0.1 - 0.9$
ψ_0	Air entry pressure (m H_2O)	$0.05 - 1.0$
K_{sat}	Saturated hydraulic conductivity (m/s)	$10^{-5} - 10^{-3}$
ϕ	Porosity (m^3/m^3)	$0.2 - 0.55$
ω	Single-scattering albedo	$0 - 0.1$
l	Correlation length (m)	$0 - 0.5$
r	RMS height (m)	$0 - 0.02$
b	Regression parameter	$0.1 - 0.3$

C. Implementation of EnKF

In this paper, the nonlinear propagator $f()$ in (5) represents the coupled LSP-DSSAT-MB model; x is the state vector consisting near-surface VSM along with T_B estimated by the MB model; u_t is the vector of meteorological forcings at time t, and θ are the model parameters in the LSP-DSSAT-MB model. The augmented state vector x_i [(11)] includes soil moisture at depths of 2 and 4 cm, T_B, and the imperfectly known parameters describing the first layer of the soil and those in the MB model (see Table III). The impact of parameters on RZSM and T_B are time-varying due to changes in the soil surface from growing vegetation. Including parameters in the state vector is an efficient approach to track their temporal behavior, provided they are sensitive to RZSM and T_B. RZSM is not included in the state vector as a lumped variable because the SVAT model requires VSMs at different nodes and would necessitate the use of correlation statistics to allocate the differences in the posterior and the prior RZSM values to changes at different

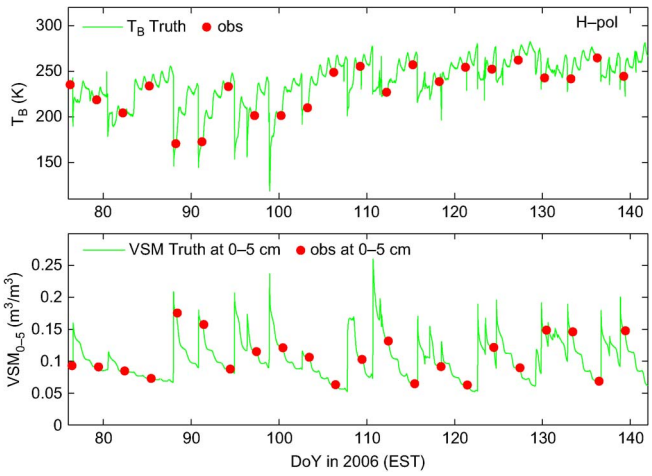

Fig. 2. Observations of T_B and VSM at 0–5 cm from the MicroWEX-5.

nodes in the soil. This seems less physically realistic than allowing the LSP model to use its embedded biophysics to propagate changes in the near surface soil moisture to lower nodes to ensure mass and energy balance over the next time step when only surface soil moisture is in the state vector. Including RZSM in the state vector is also not physically meaningful because T_B is only sensitive to the top few centimeters of the soil. Inclusion of VSM at all the 15 nodes encompassing the root zone in the state vector is also not desirable because the state vector becomes large leading to potential instabilities in the EnKF and has further been found to offer only negligible improvements to RZSM estimates [8]. The ith ensemble member is therefore expressed as

$$x_i = \begin{bmatrix} VSM_{i2cm} \\ VSM_{i4cm} \\ T_{Bi} \\ \theta_i \end{bmatrix}. \tag{11}$$

Two sets of experiments assimilating synthetic observations of T_B are performed with different parameter update scenarios. The first scenario involves the estimation of the states and all the unknown parameters listed in Table III and the second scenario involves the estimation of states and the most sensitive parameters obtained from the sensitivity studies in Section II-D. Uncertainties in the parameters that are not updated during asimilation, are still included in the experiments. The experiment using field observations of T_B from the MicroWEX-5 is conducted for the second scenario only.

The RZSM is calculated from the LSP-DSSAT model using the following equation:

$$RZSM = \frac{\sum_{i=1}^{m} VSM_i \Delta z_i}{\sum_{i=1}^{m} \Delta z_i} \tag{12}$$

where m indicates the total number of nodes (blocks) within the root zone (0–1 m), Δz_i the thickness of the ith node, and VSM_i the VSM at ith node.

One hundred ensemble members $(N = 100)$ were chosen for assimilation to achieve reliable estimates [66]. The synthetic truth was obtained from one of the realizations from an open-loop simulation of the LSP-DSSAT-MB model using perturbed precipitation forcings and perturbed parameters. Synthetic observations were obtained by adding a Gaussian error to the truth. Horizontally-polarized T_B observations were assimilated into the LSP-DSSAT-MB model every three days. The assimilation time was chosen to be at 6 A.M. EST, corresponding to the availability of current and near future remotely-sensed microwave observations [4], [5]. The truth was not included in the ensemble of 100 members during the assimilation experiments. The field observations were obtained from the MicroWEX-5 experiment (see Fig. 2), described in Section II-A and were assumed to be unbiased [67]. The RMSE between the mean estimates of RZSM and the truth along with the time-averaged standard deviations of the mean estimates (i.e., the average standard deviation: ASD) were computed to quantify algorithm performance. The RMS differences (RMSD) between the mean estimates and field observations during MicroWEX-5 and the ASD was used to quantify the filter performance. While the RMSE/RMSD is a metric of accuracy, the ASD is a metric of uncertainty and can be used as an error metric of the RMSE. The maximum expected error in the estimates is therefore calculated as the cumulative effect of the RMSE/RMSD and ASD values. An optimal estimate of RZSM would have low values of both the RMSE/RMSD and ASD.

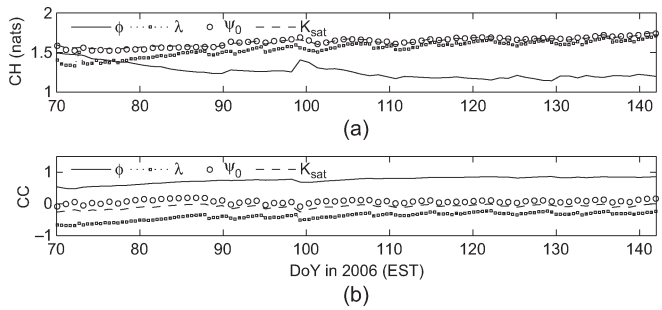

Fig. 3. (a) Conditional entropy of RZSM and (b) correlation coefficients between RZSM and the four LSP parameters over the growing season. ϕ, λ, ψ_0, and K_{sat} represent soil porosity, pore-size index, air-entry pressure, and saturated hydraulic conductivity, respectively.

$$RMSE(or)RMSD = \sqrt{\frac{1}{N_t}\sum_{t=1}^{N_t}\left(RZSM_t^{mean} - RZSM_t^{truth(or)obs}\right)^2} \tag{13}$$

$$ASD = \frac{1}{N_t}\sum_{t=1}^{N_t}\frac{1}{100}\sum_{i=1}^{100}\left(RZSM_t^{i} - RZSM_t^{mean}\right)^2 \tag{14}$$

where N_t is the number of RZSM estimates over time, $RZSM_t^{mean}$ is the mean RZSM at time t computed from the N ensemble members, and $RZSM_t^{truth}$ is the true value of the RZSM at time t for synthetic experiments and $RZSM_t^{obs}$ is the observed mean value of the RZSM at time t during MicroWEX-5.

D. Uncertainties in Forcings and Observations

In this paper, the errors in both synthetic and MicroWEX-5 observations were assumed Gaussian with zero mean. The standard deviation of the errors in T_B was 3 K. Among the forcings, a Gaussian observation error with standard deviation equal to 12% of the observed value of precipitation/irrigation was

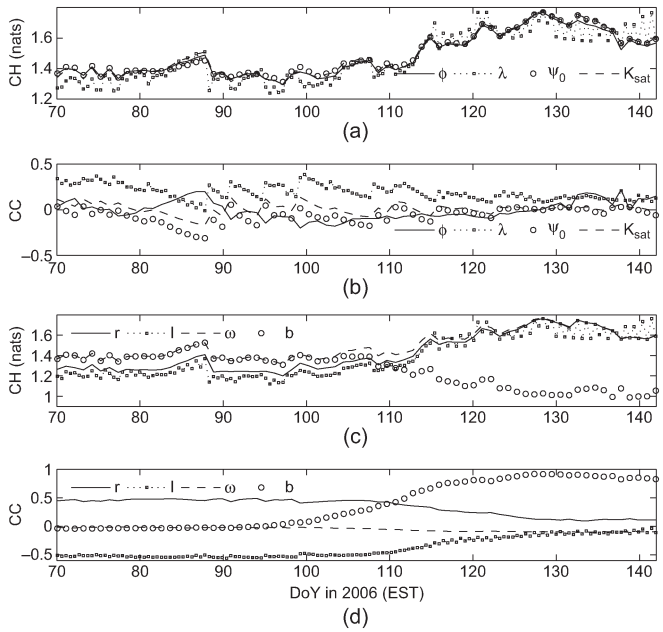

Fig. 4. (a) and (c) Conditional entropy of T_B and (b) and (d) correlation coefficients between T_B and the eight parameters in the LSP and MB models over the growing season. ϕ, λ, ψ_0, K_{sat}, r, l, ω, and b represent soil porosity, pore-size index, air-entry pressure, saturated hydraulic conductivity, root mean square height, correlation length, scattering coefficient, and vegetation parameter, respectively.

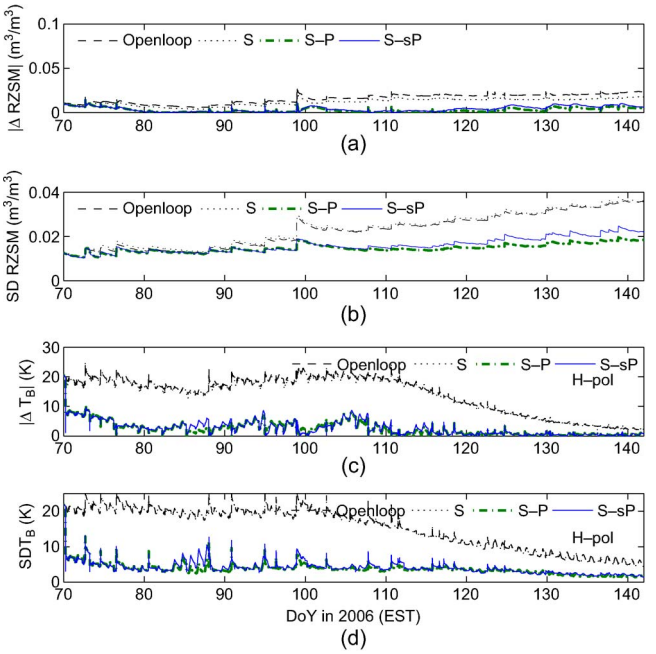

Fig. 5. Absolute errors and standard deviations between the synthetic truth and estimates of (a) and (b) RZSM and (c) and (d) T_B, respectively when synthetic observations of T_B were assimilated. S, S-P, and S-sP represents state-only, state-parameter, and state-sensitive parameter, respectively.

introduced during events [68], [69]. No errors were introduced in the absence of the events.

IV. Results and Discussion

A. Parameter Sensitivity Using Conditional Entropy

Parameters that are sensitive to RZSM and T_B should display low CH values and high correlations (CC). The CH and CC obtained for different parameters are shown in Figs. 3 and 4 for RZSM and T_B, respectively. Both CH and CC predict ϕ to be the most sensitive parameter to RZSM [see Fig. 3(a) and (b)]. A season-average CH of 1.2 nats and correlation of 0.75 are obtained for ϕ. The K_{sat} and ψ_0 are found to be the least sensitive to RZSM by both CH and CC. While λ was found to be sensitive during the early stage, with average CH and CC values of 1.4 nats and -0.5, respectively, the sensitivity decreased as the season progressed, with values reaching 1.75 nats and -0.2, respectively.

The CH and CC obtained between the soil parameters and T_B are shown in Fig. 4(a) and (b), and those obtained between the MB-model parameters and T_B are shown in Fig. 4(c) and (d). Among the soil parameters, λ was the most sensitive to T_B during the early and midstages with average CH and CC values of 1.35 nats and 0.2, respectively. Although ϕ was observed as the most sensitive soil parameter toward the end of the reproductive stage [see Fig. 4(a)], it obtained a relatively high CH value of 1.57 nats at the end of the season, indicating the low sensitivities of soil parameters to T_B during full vegetation. Both the CH and CC predict r and l to be the most sensitive MB-model parameters during the early and midseasons, with average CH values in the range of 1.25–1.30 nats and CC values in the range of 0.45–0.50. In the reproductive stage, b was found to be the most sensitive parameter with average CH and CC values of 1.05 nats and 0.85, respectively. Parameter ω was found to be insensitive to T_B by both CH and CC.

TABLE IV
Root Mean Square Errors (RMSE) and Average Standard Deviations (ASD) of (A) RZSM (m^3/m^3) and (B) T_B (K) Averaged Over the Whole Season and Over Different Growth Stages of Corn When Assimilating Synthetic Observations of T_B. The S-P Represents the Update of States and All Eight Parameters in Table III. The S-sP Represents the Update of States and Parameters λ, ϕ, r, l, and b

(A) RZSM	Open loop		S-P		S-sP	
	RMSE	ASD	RMSE	ASD	RMSE	ASD
Overall season	0.014	0.022	0.004	0.0014	0.006	0.0016
Early	0.008	0.014	0.004	0.0013	0.004	0.013
Mid	0.015	0.023	0.003	0.015	0.004	0.015
Reproductive	0.018	0.031	0.005	0.016	0.007	0.019
(B) T_B	Open loop		S-P		S-sP	
	RMSE	ASD	RMSE	ASD	RMSE	ASD
Overall season	15.4	15.4	4.6	4.2	4.7	4.6
Early	17.7	20.4	6.9	5.8	7.0	6.2
Mid	19.1	17.7	3.5	4.0	3.6	4.5
Reproductive	7.4	8.4	0.7	2.7	0.7	2.7

Based upon the CH and CC values obtained over the entire season, λ, ϕ, r, l, and b are found to be the most sensitive parameters and should be chosen for update during T_B assimilation. In general, during the early and midstages, lower CC values are obtained for T_B than for RZSM, while the CH values remained low at 1.2 nats for both T_B and RZSM. Higher sensitivities observed in the CH values for T_B are probably due to the additional higher-order information extracted by CH than CC from the nonlinear relationships between T_B and the model parameters over the growing season.

B. Identical Twin Synthetic Experiment

1) Estimation of States and Parameters: In the synthetic experiment, where most of the uncertainty and bias is

TABLE V
MEANS AND STANDARD DEVIATIONS (STD. DEV.) OF THE EIGHT PARAMETERS IN THE LSP AND MB MODELS AT THE END OF THE SEASON WHEN SYNTHETIC OBSERVATIONS OF T_B WERE ASSIMILATED

Parameter	Truth	Prior		S-P		S-sP	
		Mean	Std. dev.	Mean	Std. dev.	Mean	Std. dev.
ϕ	0.38	0.37	0.10	0.43	0.06	0.43	0.07
ψ_0	0.72	0.50	0.24	0.61	0.21	0.56	0.22
λ	0.18	0.48	0.28	0.24	0.11	0.24	0.13
K_{sat}	$7.2X10^{-4}$	$15X10^{-4}$	$3.0X10^{-4}$	$5.1X10^{-4}$	$2.5X10^{-4}$	$4.9X10^{-4}$	$3.0X10^{-4}$
r	$2.5X10^{-3}$	0.01	$6.0X10^{-3}$	$5.6X10^{-3}$	$4.1X10^{-3}$	$5.7X10^{-3}$	$4.2X10^{-3}$
l	0.12	0.25	0.15	0.30	0.10	0.30	0.10
ω	0.08	0.05	0.03	0.05	0.03	0.05	0.03
b	0.17	0.20	0.06	0.17	0.01	0.17	0.02

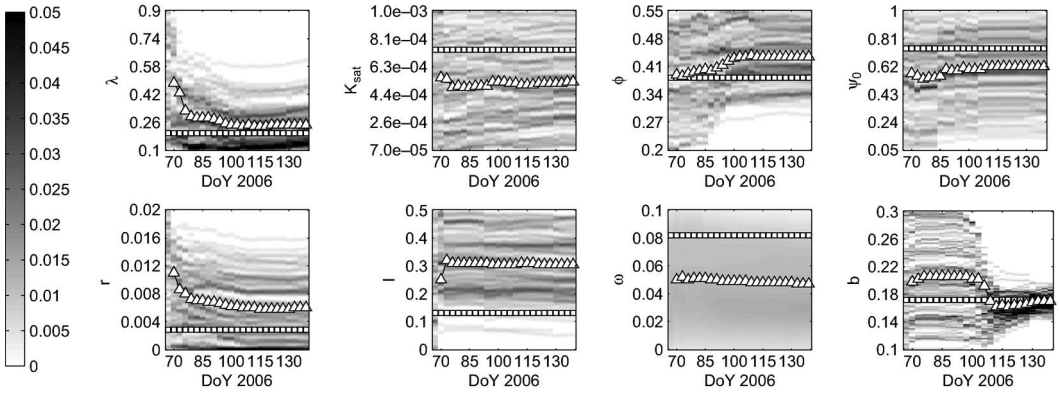

Fig. 6. Posterior distributions of pore-size index (λ), saturated hydraulic conductivity (K_{sat}), porosity (ϕ), air-entry pressure (ψ_0), RMS height (r), correlation length (l), single-scattering albedo (ω), and regression parameter (b) during the growing season for state and parameter updates when synthetic observations of T_B were assimilated. The Square and triangle markers represent the true and mean values, respectively. Grayscale bar represents the probability values of the parameters. Darker shades represent higher probabilities compared to lighter shades.

embedded in the parameters, significant improvements to RZSM estimates are obtained when parameters are updated along with the states compared to state-only estimation (see Fig. 5). Table IV(A) shows the improvements to RZSM estimates obtained when all the eight parameters in Table III are updated along with states when synthetic observations of T_B are assimilated. Fig. 5(a) and (b) show the time series of the improvement and its standard deviations during assimilation. The RMSEs of the RZSM estimates are reduced by 71.5% compared to the open loop estimates and the ASDs obtained over the entire season are around 0.014 m^3/m^3 compared to 0.022 m^3/m^3 obtained for the open loop [Table IV(A)]. Fig. 5(c) shows the absolute errors in the mean estimates of T_B obtained using EnKF. Model uncertainty decreases in the reproductive stage starting on DoY 116 because $T_{Bcanopy}$ is the primary component during this stage and includes only the b parameter that has small uncertainties, resulting in smaller errors. RMSEs and ASD in the open loop estimate themselves reduce in the reproductive stage as seen in Fig. 5(c) and (d). The mean estimates of T_B using the EnKF algorithm are closer to the truth over the entire season compared to open loop estimates. The RMSEs and ASDs of T_B estimates are reduced by 10.8 K or 70.7% over open loop estimates [see Table IV(B)]. The ASD obtained over the growing season is approximately 4.2 K compared to 15.5 K for the open loop, a reduction of over 73%.

Since model physics is assumed perfectly known [i.e., $\eta = 0$ in (5)] in the synthetic experiment, parameters that are sensitive to T_B are expected to converge to the true values. The means and SDs of the posterior estimates of the parameters are listed in Table V and the posterior PDFs are shown in Fig. 6. The mean estimates of the most sensitive soil parameters, namely λ and ϕ, converged with a difference of 33% and 11% from the true value, respectively. Parameters ψ_0 and K_{sat} are the least sensitive parameters and do not converge throughout the season as seen in Fig. 6. Amongst the MB model parameters, while r and l converged during early and midstages as seen in Fig. 6, b converged to the true value of 0.17 with a standard deviation of 0.01 during the reproductive stage (see Table V). These results also support the sensitivity analyses presented in Section IV-A using the CH and CC.

2) Estimation of States and the Most Sensitive Parameters: As inferred earlier in Section IV-A, parameters ϕ, λ, r, l, and b were selected as the most sensitive parameters to T_B. When these parameters are estimated along with the states, similar reductions in RMSEs of RZSM estimates are obtained as those when all the eight parameters are estimated [see Table IV(A)]. The RMSEs in the RZSM estimates are reduced by 57% compared to the open loop estimates when T_B is assimilated, slightly lower to that obtained when all eight parameters were updated. The RMSEs in the T_B estimates are reduced by 10.7 K or 70% compared to the open loop estimates with an ASD of 4.6 K. The only difference in the T_B estimates between updating all the eight parameters and λ, ϕ, r, c, and b are during the long dry-down periods. During such dry-down periods, for example DoY 85–88, parameter ψ_0 that displays high sensitivity to T_B [see Fig. 4(a)] is not updated leading to an increase in RMSE values as seen in Fig. 5(c). The posterior PDFs of the eight parameters are shown in Fig. 7.

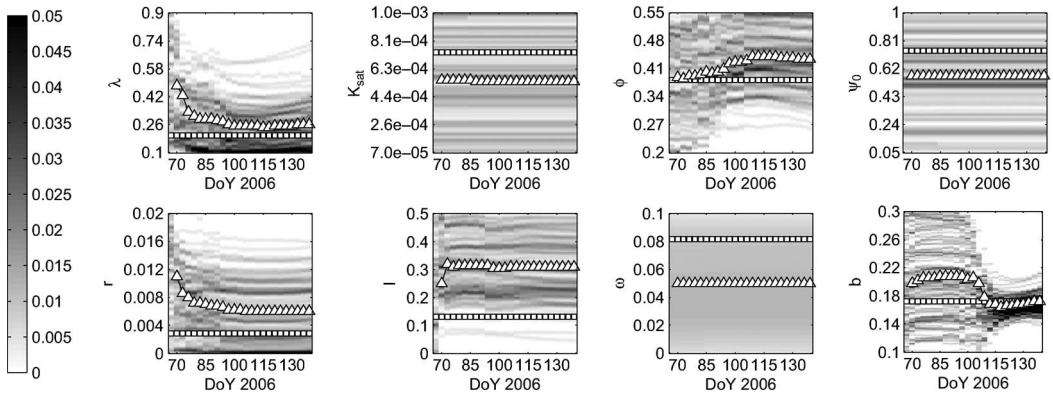

Fig. 7. Posterior distributions of pore-size index (λ), saturated hydraulic conductivity (K_{sat}), porosity (ϕ), air-entry pressure (ψ_0), RMS height (r), correlation length (l), single-scattering albedo (ω), and regression parameter (b) during the growing season for state and sensitive parameter updates when synthetic observations of T_B were assimilated. The Square and triangle markers represent the true and mean values, respectively. Grayscale bar represents the probability values of the parameters. Darker shades represent higher probabilities compared to lighter shades.

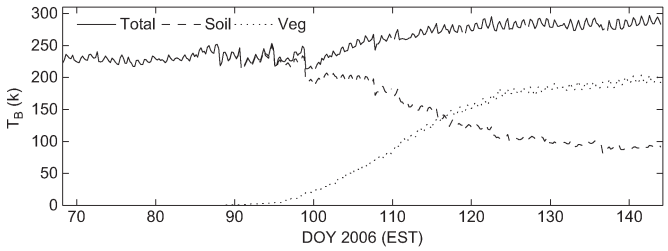

Fig. 8. Contributions from soil (T_{Bsoil}) and vegetation ($T_{Bcanopy}$) toward total T_B during a growing season of corn.

C. Assimilation Using MicroWEX-5 Observations

As mentioned earlier, additional bias may be introduced when field observations are assimilated and simultaneous state-parameter estimation can be used to address such bias in the model. Since the contributions from T_{Bsoil} and $T_{Bcanopy}$ in estimating total T_B vary as the season progresses, updating parameters that are highly sensitive to T_B during each of the three growth stages of corn is essential for the accurate estimation of RZSM. Fig. 8 shows the two components over the entire season for an open loop realization of the LSP-DSSAT-MB model. Based upon the senstivity analyzes, parameters λ, r, l, and b are chosen for update over all three growth stages (see Table I), ψ_0 during the early season, and ϕ during the mid- and reproductive seasons. Parameter ψ_0 shows high sensitivity during long dry-down periods under bare-soil conditions, as seen in Fig. 4(a), and is updated during the early season. Although the contribution from T_{Bsoil} decreases during the mid- and reproductive stages, soil parameter ϕ shows increased sensitivity to RZSM and T_B as seen in Figs. 3(a) and (b) and 4(b), respectively. Parameters r and l that describe the soil roughness influence the estimation of T_B contributed from soil which still accounts to approximately one-third of overall T_B during the reproductive stage (see Fig. 8) and hence retained throughout the season.

Table VI shows the improvements to RZSM and T_B estimates obtained when MicroWEX-5 observations of T_B are assimilated. The absolute errors between the RZSM estimates and the observations and the ASDs in the estimates are shown in Fig. 9(a) and (b). Fig. 9(c) and (d) show the absolute errors in the estimates of T_B and the standard deviations during assimilation. The RMSDs in T_B and RZSM estimates are reduced by 5.4 K or 22.5% and 15.4%, respectively, compared to open loop estimates over the entire season. Assimilation also reduces uncertainty in the estimates of T_B and RZSM with ASDs of 7.6 K and 0.014 m^3/m^3, respectively, compared to ASDs of 14.8 K and 0.024 m^3/m^3 obtained in the open loop. The RMSEs obtained in this study are moderately better than those obtained in previous studies. RMSEs of 0.023 m^3/m^3 and 0.04 m^3/m^3 in RZSM estimates were reported in [11] and [7], respectively, when real observations of T_B were assimilated under static vegetation conditions. In [70], an RMSE of 0.03 m^3/m^3 and ASD of 0.02 m^3/m^3 in RZSM estimates was reported when near-surface soil moisture was assimilated under dynamic vegetation conditions similar to that in this study. While only moderate improvements in RMSDs are observed over the entire season, variations in performance can be observed within the season.

During the early stage (DoY 76–95), the RMSDs and ASD in the RZSM estimates are reduced by 33.3% and 13.3% over open loop estimates. The RMSDs and ASD in T_B estimates are reduced by 15.1% and 40.4% over open loop estimates [see Fig. 9(a) and (b)]. Although the model estimates from assimilation are closer to the MicroWEX-5 observations than the open loop estimates, reduced improvements are observed during and immediately following precipitation/irrigation events. The IEM model overestimates T_B during precipitation/irrigation events and underestimates T_B during initial dry-down periods leading to a smaller dynamic range in the estimates of T_B. Similar to T_B estimates, maximum errors in RZSM estimates are also observed immediately following such events. If the RMSDs in T_B estimates are computed over times excluding 12 h following precipitation/irrigation events, a reduction of 22.2% is obtained with an ASD of 7.8 K. The reduced performance during precipitation events is due to the suboptimal estimates of dielectric constant in the MB model. As mentioned earlier, the four-component model [71] was used to compute the dielectric constant in this study. Errors in dielectric constant arise during precipitation/irrigation events because of inaccuracies in the estimates of the four components, namely soil solids, air, free water, and bound water. In such cases, updating only

TABLE VI
ROOT MEAN SQUARE DIFFERENCES (RMSD) AND AVERAGE STANDARD DEVIATIONS (ASD) OF T_B (K) AND RZSM (m^3/m^3) AVERAGED OVER THE ENTIRE SEASON AND OVER DIFFERENT GROWTH STAGES OF CORN WHEN MICROWEX-5 OBSERVATIONS OF T_B WERE ASSIMILATED

Growth stage	T_B (K)				RZSM (m^3/m^3)			
	Open loop		EnKF		Open loop		EnKF	
	RMSD	ASD	RMSD	ASD	RMSD	ASD	RMSD	ASD
Overall season	24.0	14.8	18.6	7.6	0.026	0.024	0.022	0.014
Early	21.8	20.3	18.5	12.1	0.006	0.015	0.004	0.013
Mid	20.6	18.0	21.0	5.7	0.021	0.023	0.020	0.011
Reproductive	27.7	8.4	16.3	4.2	0.036	0.031	0.030	0.016

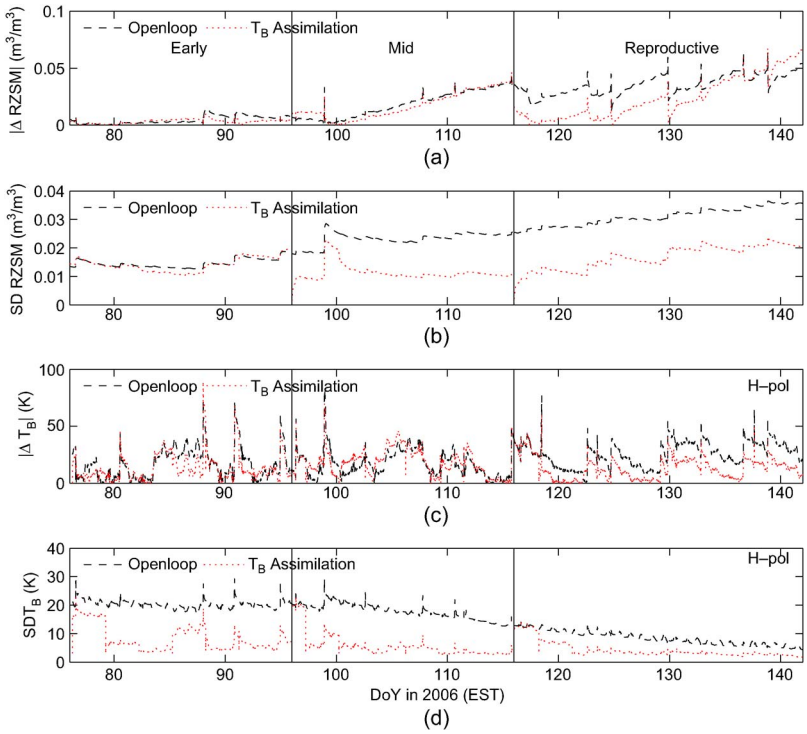

Fig. 9. Absolute errors between the observations and estimates of (a) RZSM and (c) T_B and the SD in the estimates of (c) RZSM and (d) T_B when MicroWEX-5 observations of T_B were assimilated.

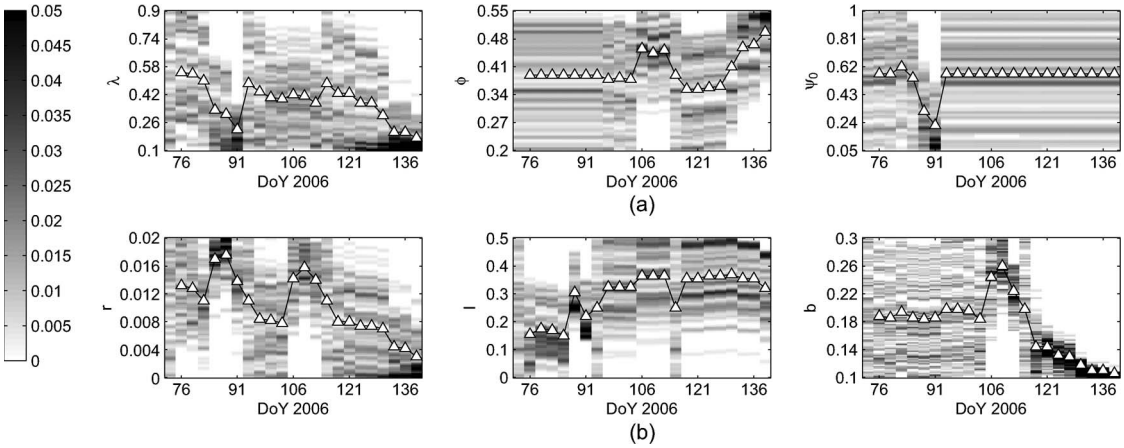

Fig. 10. Posterior distributions of (a) Porosity (ϕ), pore-size index (λ), and air-entry pressure (ψ_0) and (b) RMS height (r), correlation length (l), and b parameter when MicroWEX-5 observations of T_B were assimilated. The triangle markers represent the mean values. Grayscale bar represents the probability values of the parameters. Darker shades represent higher probabilities compared to lighter shades.

the soil roughness parameters, r and l, immediately following precipitation/irrigation events may be insufficient for the accurate estimation of T_B. When assimilation is performed near a precipitaion event (DoY 88), although the EnKF improves T_B estimates at the time of assimilation by significantly changing the values of r and l as shown in Fig. 10(b), the model estimates move farther away from the truth immediately after assimilation. Parameter ψ_0 is most sensitive to T_B from DoY 85–88 and displays maximum convergence over these times during assimilation, as seen in Fig. 10(a).

During the midstage (DoY 96–115), only a moderate reduction in RMSD of 4.8% is observed in RZSM estimates compared to the open loop (see Table VI). Although the ASD in T_B estimates is reduced from 18 K to 5.7 K, reductions of RMSDs in T_B estimates are not observed. The reduced performance is attributed to complexities in estimating T_B by a highly dynamic vegetation during this stage. The contribution from the canopy gradually increases, while the contribution from the soil decreases with increasing vegetation (see Fig. 8). The mean estimates of the b parameter, used for computing $T_{Bcanopy}$ also increase over this stage as seen in Fig. 10(b), but are insufficient to capture the dynamic variations in T_B. The senstivities of r and l to T_B decrease, as expected, and are indicated by their reduced convergence in Fig. 10(b).

During the reproductive stage (DoY 116–142), reduction in RMSD of 16.7% is observed in RZSM estimates compared to the open loop. Maximum improvements, in terms of RMSD reductions in T_B estimates are observed. The RMSDs in T_B estimates are reduced by 11.4 K or 41.2% compared to the open loop and the ASD is reduced by 4.2 K. The open loop estimates of T_B in the reproductive stage indicate the presence of a model bias of 12 K, as shown in Fig. 9(c). Updating the b parameter helps remove most of this bias. Although contribution from the canopy is the most significant during the reproductive stage, the soil contribution is approximately one-third of the total predicted T_B. Due to the soil contribution, reduced improvements in T_B estimates are observed following precipitation/irrigation events [see Fig. 9(c)] due to suboptimal VSM estimated by the LSP model following such events similar to that observed in the early stage. However, in comparison to the estimates of T_B obtained during end of dry-downs in the early stage, estimates of T_B during the reproductive stage are much closer to the observations due to the reduced contribution of soil to overall T_B. The estimates of T_B also move farther away from the observations after DoY 130 when there has been significant ear growth (specific weight of ears on DoY 131 were observed at 1 kg/m^2). The deviation of T_B estimates from the observation beyond DoY 131 is likely because the optical depth in (1) is computed based on a simplistic linear equation parameterized by b. Such a simplistic equation is inadequate in assimilation scenarios to capture the complexities in T_B caused by ear formation. Significant RMSD reductions in RZSM estimates of 61.2% compared to open loop estimates are obtained prior to Doy 131 as seen in Fig. 9(a).

V. Summary and Conclusion

In this paper, L-band microwave observations were assimilated using the EnKF to improve RZSM estimates from a coupled SVAT-vegetation model linked to a forward microwave model under dynamic land surface conditions. Simultaneous state-parameter updates were performed by assimilating both synthetic and field observations during a growing season of sweet corn.

The sensitivities of parameters to the states were investigated by using the information-theoretic measure of CH and the traditional second-order metric of CC. While both CH and CC offered similar sensitivities for parameters with respect to RZSM, the CH metric provided better separation amongst the parameters in terms of their sensitivity to T_B than CC. This is potentially due to the additional higher order information extracted by CH than CC from the nonlinear relationships between T_B and the parameters over the growing season. Among the soil parameters, λ was the most sensitive to T_B during the early and midseasons, while porosity ϕ was more sensitive in the reproductive stage. In the microwave model, the soil roughness parameters, r and l were the most sensitive during the early and midseasons, while the vegetation parameter, b, was the most sensitive during the reproductive stage.

Assimilation offered significant reductions in RMSE/RMSD and ASD in the synthetic case and marginal improvements in the MicroWEX-5 case compared to the open loop. In the synthetic case, assimilation provided RMSE reductions of 70% compared to the open loop estimates. Low RMSEs of 0.005 m^3/m^3 indicate the absence of model bias in estimating RZSM by directly assimilating T_B into the LSP-DSSAT-MB model as against retrieving soil moisture from observations of T_B and then assimilating the retrieved soil moisture into the LSP model. When the most sensitive parameters were estimated along with the states, similar reductions in RMSEs of RZSM estimates were obtained as those when all the eight parameters were estimated. Identifying the most sensitive parameters and estimating them during assimilation can provide similar improvements to RZSM estimates, while reducing the occurrence of equifinality and computational complexities.

In contrast to the synthetic case, significant differences in RZSM estimates were observed between different stages of corn growth when field observations of T_B were assimilated. Maximum RMSD reductions in RZSM estimates of 33.3% were observed compared to open loop estimates in the early stages, while reduced improvements of 4.8% and 16.7% were observed in the mid- and reproductive stages, respectively. Maximum errors in T_B estimates in the early season were observed during and immediately following precipitation/irrigation events. The IEM model overestimates T_B during precipitation/irrigation events and underestimates T_B during initial dry-down periods leading to a smaller dynamic range in the estimates of T_B, particularly under baresoil conditions. While the optimization of soil roughness parameters through assimilation reduces the error, improved estimation of emissivity these periods is required for further improvements in the estimation of T_B. Significant errors in T_B estimates were observed during the midstage of corn growth and after ear formation. The linear vegetation model used for estimating canopy opacity did not capture the complexities in T_B, particularly during high dynamic growth and ear formation. Since the canopy component contributing to overall T_B is primarily driven by the distribution of moisture in the canopy, a canopy opacity model that is based upon vertical profiles of moisture content within the crop will improve estimates of T_B during the mid- and reproductive stages of crop growth. In addition, estimating both soil and vegetation parameters in the coupled LSP-DSSAT model may result in better growth and development of the vegetation, further improving the T_B estimates.

ACKNOWLEDGMENT

The authors acknowledge computational resources and support provided by the University of Florida High-Performance Computing Center for all the model simulations conducted in this study.

REFERENCES

[1] J. Hanson, K. Rojas, and M. Schaffer, "Calibrating the root zone water quality model," *Agronomy J.*, vol. 91, no. 2, pp. 171–177, 1999.

[2] W. Crow, W. Kustas, and J. Prueger, "Monitoring root-zone soil moisture through the assimilation of a thermal remote sensing-based soil moisture proxy into a water balance model," *Remote Sens. Environ.*, vol. 112, no. 4, pp. 1268–1281, 2008.

[3] R. Reichle, W. Crow, and C. Kepenne, "An adaptive Ensemble Kalman filter for soil moisture data assimilation," *Water Res. Res.*, vol. 44, no. W03423, 2008. doi:10.1029/2007WR006357.

[4] Y. Kerr, P. Waldteufel, J. Wigneron, J. Martinuzzi, J. Font, and M. Berger, "Soil moisture retrieval from space: The Soil Moisture and Ocean Salinity (SMOS) Mission," *IEEE Trans. Geosci. Remote Sens.*, vol. 39, no. 8, pp. 1729–1735, Aug. 2001.

[5] D. Entekhabi, E. Njoku, P. O'Neill, M. Spencer, T. Jackson, J. Entin, E. Im, and K. Kellogg, "The Soil Moisture Active/Passive Mission (SMAP)," in *Proc. IGARSS*, 2008, vol. 3, pp. III-1–III-4.

[6] N. R. Council, Earth Science and Applications From Space: National Imperatives for the Next Decade and Beyond, 2007.

[7] C. Huang, X. Li, and J. Gu, "Experiments of one-dimensional soil moisture assimilation system based on ensemble Kalman filter," *Remote Sens. Environ.*, vol. 112, no. 3, pp. 888–900, 2008.

[8] A. Monsivais-Huertero, W. Graham, J. Judge, and D. Agrawal, "Effect of simultaneous state-parameter estimation and forcing uncertainties on root-zone soil moisture for dynamic vegetation using EnKF," *Adv. Water Resour.*, vol. 33, no. 4, pp. 468–484, 2010.

[9] V. Pauwels, N. Verhoest, G. De Lannoy, V. Guissard, C. Lucau, and P. Defourny, "Optimization of a coupled hydrology-crop growth model through the assimilation of observed soil moisture and leaf area index using an ensemble Kalman filter," *Water Res. Res.*, vol. 43, no. W04421, pp. 1–17, 2007. doi:10.1029/2006WR004942.

[10] H. Moradkhani, S. Sorooshina, H. Gupta, and P. Houser, "Dual state-parameter estimation of hydrological models using Ensemble Kalman filter," *Adv. Water Res.*, vol. 28, no. 2, pp. 135–147, 2005.

[11] W. Crow and E. Wood, "The assimilation of remotely sensed soil brightness temperature imagery into a land surface model using Ensemble Kalman filtering: A case study based on ESTAR measurements during SGP97," *Adv. Water Resour.*, vol. 26, no. 2, pp. 137–149, 2003.

[12] R. Reichle, J. Walker, R. Koster, and P. Houser, "Extended versus Ensemble Kalman filtering for land data assimilation," *J. Hydrometeorol.*, vol. 3, no. 6, pp. 728–740, 2002.

[13] R. Reichle, D. McLaughlin, and D. Entekhabi, "Hydrologic data assimilation with the Ensemble Kalman filter," *Mon. Weather Rev.*, vol. 130, no. 1, pp. 103–114, Jan. 2002.

[14] S. Margulis, D. McLaughlin, D. Entekhabi, and S. Dunne, "Land data assimilation and estimation of soil moisture using measurements from the Southern Great Plains 1997 field experiment," *Water Res. Res.*, vol. 38, no. 12, pp. 35-1–35-18, 2002. doi:10.1029/2001WR001114.

[15] J. Qin, S. Liang, K. Yang, I. Kaihotsu, R. Liu, and T. Koike, "Simultaneous estimation of both soil moisture and model parameters using particle filtering method through the assimilation of microwave signal," *J. Geophys. Res.*, vol. 114, no. D15, pp. 1–13, 2009. doi:10.1029/2008JD011358.

[16] X. Han and X. Li, "An evaluation of the nonlinear/non-gaussian filters for the sequential data assimilation," *Remote Sens. Environ.*, vol. 112, no. 4, pp. 1434–1449, Apr. 2008.

[17] Y. Zhou, D. McLaughlin, and D. Entekhabi, "Assessing the performance of the ensemble Kalman Filter for land surface data assimilation," *Mon. Weather Rev.*, vol. 134, no. 8, pp. 2128–2142, Aug. 2006.

[18] W. Ni-Meister, "Recent advances on soil moisture data assimilation," *Phys. Geogr.*, vol. 29, no. 1, pp. 19–37, 2008.

[19] H. Gao, E. F. Wood, M. Drusch, W. Crow, and T. J. Jackson, "Using a microwave emission model to estimate soil moisture from ESTAR observations during SGP99," *J. Hydrometeorol.*, vol. 5, no. 1, pp. 49–63, Feb. 2004.

[20] S. Dunne, D. Entekhabi, and E. G. Njoku, "Impact of multiresolution active and passive microwave measurements on soil moisture estimation using the Ensemble Kalman smoother," *IEEE Trans. Geosci. Remote Sens.*, vol. 45, no. 4, pp. 1016–1028, Apr. 2007.

[21] T. Chen, J. Morris, and E. Martin, "Particle filters for state and parameter estimation in batch processes," *J. Process Control*, vol. 15, no. 6, pp. 655–673, Sep. 2005.

[22] G. De Lannoy, P. Houser, V. Pauwels, and N. Verhoest, "State and bias estimation for soil moisture profiles by an ensemble Kalman filter: Effect of assimilation depth and frequency," *Water Res. Res.*, vol. 43, no. W06401, 2007. doi:10.1029/2006WR005100.

[23] K. Beven, "A manifesto for the equifinality thesis," *J. Hydrol.*, vol. 320, no. 1/2, pp. 18–36, Mar. 2006.

[24] Y. Luo, E. Weng, X. Wu, C. Gao, X. Zhou, and L. Zhang, "Parameter identifiability, constraint, and equifinality in data assimilation with ecosystem models," *Ecolog. Appl.*, vol. 19, no. 3, pp. 571–574, Apr. 2009.

[25] J. Casanova, F. Yan, M. Jang, J. Fernandez, J. Judge, C. Slatton, K. Calvin, T. Lin, O. Lanni, and L. W. Miller, Field Observations During the Fifth Microwave, Water, and Energy Balance Experiment (MicroWEX-5): From March 9 Through May 2006. Circular no. 1514, Center Remote Sens., Univ. Florida, Gainesville, FL, Tech. Rep. Circular 1514. [Online]. Available: http://edis.ifas.ufl.edu/AE407

[26] J. Judge, A. England, J. Metcalfe, D. McNichol, and B. Goodison, "Calibration of an integrated land surface process and radiobrightness (LSP/R) model during summertime," *Adv. Water Res.*, vol. 31, no. 1, pp. 189–202, 2008.

[27] J. Judge, L. Abriola, and A. England, "Numerical validation of the land surface process component of an LSP/R model," *Adv. Water Res.*, vol. 26, no. 7, pp. 733–746, Jul. 2003.

[28] J. Judge, A. England, W. Crosson, B. Hornbuckle, W. Boprie, E. Kim, and Y. Lieu, "A growing season land surface process/radiobrightness model for wheat-stubble in the Southern Great Plains," *IEEE Trans. Geosci. Remote Sens.*, vol. 37, no. 5, pp. 2152–2158, Sep. 1999.

[29] B. Whitfield, J. Jacobs, and J. Judge, "Intercomparison study of the land surface process model and the common land model for a prairie wetland in Florida," *J. Hydrometeorol.*, vol. 7, no. 6, pp. 1247–1258, 2006.

[30] Y. Chung, "A snow-soil-vegetation-atmosphere-transfer/radiobrightness model for wet snow," Ph.D. dissertation, Univ. Michigan, Ann Arbor, MI, 2007.

[31] S. Verseghy, N. McFarlane, and M. Lazare, "Class-A Canadian land surface scheme for GCMs, II. Vegetation model and coupled runs," *Int. J. Climatol.*, vol. 13, no. 4, pp. 347–370, May/Jun. 1993.

[32] K. Trenberth, *Climate System Modeling*. New York: Cambridge Univ. Press, 1995.

[33] J. Peixoto and A. Oort, *Physics of Climate*. New York: Amer. Inst. Phys., 1992.

[34] J. Philip and D. de Vries, "Moisture movement in porous materials under temperature gradients," *Trans. Amer. Geophys. Union*, vol. 38, no. 2, pp. 222–232, 1957.

[35] D. de Vries, "Simultaneous transfer of heat and moisture in porous media," *Trans. Amer. Geophys. Union*, vol. 39, no. 5, pp. 909–916, 1958.

[36] J. Casanova and J. Judge, "Estimation of energy and moisture fluxes for dynamic vegetation using coupled SVAT and crop-growth models," *Water Res. Res.*, vol. 44, p. W07 415, Jul. 2008. doi:10.1029/2007WR006503.

[37] J. Jones, G. Hoogenboom, C. Poter, K. Boote, W. Batchelor, L. Hunt, P. Wilkens, U. Singh, A. Gijsman, and J. Ritchie, "The DSSAT cropping system model," *Eur. J. Agronomy*, vol. 18, no. 3–4, pp. 235–265, Jan. 2003.

[38] C. Jones and J. Kiniry, *CERES-Maize: A Simulation Model of Maize Growth and Development*. College Stattion, TX: Texas A&M University Press, 1986.

[39] K. Boote, J. Jones, G. Hoogenboom, and G. Wilkerson, *Evaluation of the CROPGRO-Soybean Model Over a Wide Range of Experiments*. Boston, MA: Kluwer, 1997.

[40] K. Boote and J. Jones, *Simulation of Crop Growth*. New York: Marcel Dekker, 1998.

[41] S. Jagtap and J. Jones, "Adaptation and evaluation of the CROPGRO-soybean model to predict regional yield and production," *Agriculture, Ecosyst. Environ.*, vol. 93, no. 1–3, pp. 73–85, Dec. 2002.

[42] T. Mavromatis, K. Boote, J. Jones, G. Wilkerson, and G. Hoogenboom, "Repeatability of model genetic coefficients derived from soybean performance trials across different states," *Crop Sci.*, vol. 42, no. 1, pp. 76–89, Jan. 2002.

[43] J. Dardanelli, M. Calmon, J. Jones, J. Andriani, M. Diaz, and D. Collino, "Use of a crop model to evaluate soil impedance and root clumping effects on soil water extraction in three argentine soils," *Trans. ASAE*, vol. 46, no. 4, pp. 1265–1275, 2003.

[44] R. Braga and J. Jones, "Using optimization to estimate soil inputs of crop models for use in site-specific management," *Trans. ASAE*, vol. 47, no. 5, pp. 1821–1831, 2004.

[45] J. Lizaso, W. Batchelor, K. Boote, M. Westgate, P. Rochette, and A. Moreno-Sotomayor, "Evaluating a leaf-level canopy assimilation model linked to ceres-maize," *J. Agronomy*, vol. 97, no. 3, pp. 734–740, 2005.
[46] G. Alagarswamy, K. Boote, L. Allen, and J. Jones, "Evaluating the CROPGRO-soybean model ability to simulate photosynthesis response to carbon dioxide levels," *J. Agronomy*, vol. 98, no. 1, pp. 34–42, 2006.
[47] J. Timsina, K. Boote, and S. Duffield, "Evaluating the CROPGRO Soybean model for predicting impacts of insect defoliation and depodding," *J. Agronomy*, vol. 99, no. 1, pp. 148–157, 2007.
[48] J. Casanova, J. Judge, and J. Jones, "Calibration of the CERES-Maize model for linkage with a microwave remote sensing model," *Trans. ASABE*, vol. 49, no. 3, pp. 783–792, 2006.
[49] F. Ulaby, R. Moore, and A. Fung, *Microwave Remote Sensing: Active and Passive*, vol. I. Boston, MA: Artech House, 1981.
[50] T. Jackson, T. Schmugge, and J. Wang, "Passive microwave remote sensing of soil moisture under vegetation canopies," *Water Res. Res.*, vol. 18, no. 4, pp. 1137–1142, 1982.
[51] A. Fung, Z. Li, and K. Chen, "Backscattering from a randomly rough dielectric surface," *IEEE Trans. Geosci. Remote Sens.*, vol. 30, no. 2, pp. 356–369, Mar. 1992.
[52] F. Ulaby, R. More, and A. Fung, *Microwave Remote Sensing: Active and Passive. Vol. III*. Boston, MA: Artech House, 1986.
[53] T. Jackson and P. ONeill, "Attenuation of soil microwave emissivity by corn and soybeans at 1.4 and 5 GHz," *IEEE Trans. Geosci. Remote Sens.*, vol. 28, no. 5, pp. 978–980, Sep. 1990.
[54] T. Jackson and T. Schmugge, "Vegetation effects on the microwave emission of soils," *Remote Sens. Environ.*, vol. 36, no. 3, pp. 203–212, Jun. 1991.
[55] D. Le Vine and M. Karam, "Dependency of attenuation in a vegetation canopy on frequency and plant water content," *IEEE Trans. Geosci. Remote Sens.*, vol. 34, no. 5, pp. 1090–1094, Sep. 1996.
[56] J. Principe, D. Xu, and J. Fisher, *Information Theoretic Learning, in Unsupervised Adaptive Filtering*. New York: Wiley, 2010.
[57] K. Nagarajan, C. Krekeler, K. C. Slatton, and W. D. Graham, "A scalable approach to fusing spatiotemporal data to estimate streamflow via a Bayesian network," *IEEE Trans. Geosci. Remote Sens.*, vol. 48, no. 10, pp. 3720–3732, Oct. 2010.
[58] R. Duda, P. Hart, and D. Stork, *Pattern Classification*. New York: Wiley, 2001.
[59] B. Silverman, *Density Estimation for Statistics and Data Analysis*. London, U.K.: Chapman & Hall, 1986.
[60] A. Gelb, *Applied Optimal Estimation*. Cambridge, MA: MIT Press, 1974.
[61] G. Evensen, "The ensemble Kalman filter: Theoretical formulation and practical implementation," *Ocean Dyn.*, vol. 53, no. 4, pp. 343–367, 2003.
[62] A. Chanzy, M. Mumen, and G. Richard, "Accuracy of top soil moisture simulation using a mechanistic model with limited soil characterization," *Water Res. Res.*, vol. 44, no. 3, p. W03 432, Mar. 2008.
[63] D. Agrawal, A. Monsivais-Huertero, W. Graham, and J. Judge, "Parameter sensitivity analysis for root zone soil moisture in svat models," in *Proc. Amer. Geophys. Union*, Fort Lauderdale, FL, 2008, Joint Assembly.
[64] Y. Oh, K. Sarabandi, and F. Ulaby, "An empirical model and an inversion technique for radar scattering from bare soil surfaces," *IEEE Trans. Geosci. Remote Sens.*, vol. 30, no. 2, pp. 370–381, Mar. 1992.
[65] M. Zribi and M. Dechambre, "A new empirical model to retrieve soil moisture and roughness from C-band radar data," *Remote Sens. Environ.*, vol. 84, no. 1, pp. 42–52, Jan. 2003.
[66] G. van Delft, G. El Serafy, and A. Heemink, "The Ensemble Particle Filter (EnPF) in rainfall-runoff models," *Stoch. Environ. Res. Risk Assess.*, vol. 1, 2009. doi:10.1007/s00 477-008-0301-z.
[67] A. Lorenc and O. Hammon, "Objective quality control of observations using Bayesian methods: Theory, and a practical implementation," *Q. J. R. Meteorol. Soc.*, vol. 23, no. 8, pp. 1203–1211, Jan. 1988.
[68] G. Ciach, "Local random errors in tipping-bucket rain gauge measurements," *J. Atmos. Ocean. Technol.*, vol. 20, no. 5, pp. 752–759, May 2003.
[69] E. Habib, W. Krajewski, and A. Kruger, "Sampling errors of tipping-bucket rain gauge measurements," *J. Hydrol. Eng.*, vol. 6, no. 2, pp. 159–166, Mar./Apr. 2001.
[70] J. M. Sabater, L. Jarlan, J.-C. Calvet, and F. Bouyssel, "From near-surface to root-zone soil moisture using different assimilation techniques," *J. Hydrometeorol.*, vol. 8, no. 2, pp. 194–206, Apr. 2008.
[71] F. Ulaby and M. El-Rayes, "Microwave dielectric spectrum of vegetation, Part II: Dual dispersion model," *IEEE Trans. Geosci. Remote Sens.*, vol. GE-25, no. 5, pp. 550–557, Sep. 1987.
[72] J. Goudriaan, *Crop Micrometeorology: A Simulation Study*, 1st ed. Wageningen, The Netherlands: Centre Agricultural Publ. and Documentation, 1977.
[73] C. Rossi and J. Nimmo, "Modeling of soil water retention from saturation to oven dryness," *Water Res. Res.*, vol. 30, no. 3, pp. 701–708, 1994.

Karthik Nagarajan (S'00–M'09) received the B.E. degree in electronics and communication engineering from the University of Madras, Chennai, India, in 2003, and the Ph.D. and M.S. degrees in electrical engineering from the University of Florida, Gainesville, in 2005 and 2009, respectively, while simultaneously working for the Adaptive Signal Processing Laboratory and the National Science Foundation Center for High-Performance Reconfigurable Computing.

He is currently a Postdoctoral Associate with the Center for Remote Sensing, University of Florida. His research interests are in remote sensing, data fusion, pattern recognition, information theory, graphical models, multiscale estimation, and high-performance and reconfigurable computing.

Jasmeet Judge (S'94–M'00–SM'05) received the Ph.D. degree in electrical engineering and atmospheric, oceanic, and space sciences from the University of Michigan, Ann Arbor, in 1999.

She is currently the Director of the Center for Remote Sensing and an Associate Professor in Agricultural and Biological Engineering Department at the Institute of Food and Agricultural Sciences, University of Florida, Gainesville. Her research interests are in microwave remote sensing applications to terrestrial hydrology, modeling of energy and moisture interactions at the land surface and in the vadose zone, spatial and temporal scaling of remotely sensed observations, and data assimilation.

Alejandro Monsivais-Huertero received the B.S. degree in telecommunications engineering from the National Autonomous University of Mexico, Mexico City, Mexico, in 2002 and the M.S. degree in microwaves and optical telecommunications and the Ph.D. degree in electrical engineering from the University of Toulouse, Toulouse, France, in 2004 and 2007, respectively.

From 2004 to 2006, he was with the Antennes, Dispositifs et Matériaux Micro-ondes Laboratory, and from 2006 to 2007, with the Laboratoire d'Etudes et de Recherche en Imagerie Spatiale et Médicale, both at the University of Toulouse. From 2008 to 2009, he was working as a Postdoctoral Research Associate with the Center for Remote Sensing, Department of Agricultural and Biological Engineering, University of Florida, Gainesville. He is currently at the National Polytechnic Institute of Mexico, Mexico City, as a Research Professor. His research areas of interest are in microwave and millimeter-wave radar remote sensing, electromagnetic wave propagation, and retrieval algorithms.

Wendy D. Graham received the Ph.D. degree in civil engineering from the Massachusetts Institute of Technology, Cambridge, in 1989.

She is currently the Director of the Water Institute and the Carl S. Swisher Chair in Water Resources in the Agricultural and Biological Engineering Department at the University of Florida, Gainesville. Her research interests are in coupled hydrologic-water quality-ecosystem modeling; water resources evaluation and remediation; evaluation of impacts of agricultural production on surface and groundwater quality; and evaluation of impacts of climate variability and climate change on water resources, stochastic modeling and data assimilation.